Tolerable magnitudes for induced seismicity at offshore carbon capture and storage projects

James P. Verdon[1*], Ryan Schultz[2], Benjamin Edwards[3]

1. School of Earth Sciences, University of Bristol, Bristol, United Kingdom. Orcid: 0000-0002-8410-2703.
2. Swiss Seismological Service, ETH Zürich, Zürich, Switzerland. Orcid: 0000-0002-1796-9622.
3. School of Environmental Sciences, University of Liverpool, Liverpool, United Kingdom. Orcid: 0000-0001-5648-8015.

* Corresponding Author. Email: James.Verdon@bristol.ac.uk, Tel: 0044 117 331 5135.

Keywords

Induced seismicity; ground motions, tolerable magnitudes, carbon capture and storage, North Sea

Acknowledgements

James Verdon and Ben Edwards' contributions to this study were funded by the Natural Environment Research Council (NERC) under the SeisGreen Project (Grant No. NE/W009293/1). JPV was also funded by the BOPS project. Ryan Schultz was funded by the Swiss National Science Foundation under project number TMPFP2_224393, the Seisomogenic Fault Injection Test (SFIT).

Declaration of Competing Interests

JPV leads the Bristol and Oxford Passive Seismic (BOPS) project. BOPS is funded by a range of operating and oilfield service companies, many of whom are currently in the process of developing CCS projects around the UK and elsewhere. JPV and BE have acted and continue to act as independent consultants for a variety of organisations including hydrocarbon operating companies and governmental organisations on issues pertaining to induced seismicity. None of these organisations had any input into the conception, development, or analyses presented in this study.

ABSTRACT

Induced seismicity is a risk that must be managed during the development of Carbon Capture and Storage (CCS) projects. A key step in effective management of induced seismicity is the definition of a tolerable magnitude threshold, M_{TOL}*, which defines the level at which the nuisance or damage caused by induced seismicity is likely to no longer be tolerated by affected populations. Having established* M_{TOL}*, induced seismicity mitigation strategies can be implemented with the objective to avoid induced events that exceed* M_{TOL}*. In this study our objective is to estimate* M_{TOL} *for CCS developments in the waters around the UK. Siting CCS operations offshore reduces, but does not eliminate, the risks posed by induced seismicity by increasing the distance from exposed populations. For a given induced earthquake location and magnitude, we use ground motion models, nuisance and fragility functions, and population densities, to estimate the numbers of households that would experience different levels of disturbance and damage. We use past cases of induced seismicity that were, or were not, accepted by the public to define risk tolerances based on the numbers of households that experience different levels of disturbance or damage. We sense-check our results through comparison with observed macroseismic impacts from past, natural earthquakes located in the seas around the UK. As expected, we find that the strongest control on* M_{TOL} *is the distance to the shore from the proposed project. Our results can be used by CCS operators and regulators in designing induced seismicity mitigation strategies for their sites.*

1. INTRODUCTION

Carbon capture and storage (CCS) entails the capture of CO_2 at large power generation and industrial facilities and its subsequent storage in suitable geological repositories. CCS is seen as a key technology for meeting net zero targets for many industrialised nations (e.g., BEIS, 2021; Jones and Lawson, 2022). However, the injection of large volumes of CO_2 into the subsurface carries the risk of causing induced seismicity (Zoback and Gorelick, 2012; Verdon, 2014): this risk must be managed to ensure the successful development of a CCS industry.

Other industries that create subsurface perturbations have experienced induced seismicity, including conventional hydrocarbon production (e.g., Segall, 1989), geothermal energy (e.g., Zang et al., 2014), hydraulic fracturing (e.g., Schultz et al., 2020a), wastewater disposal (e.g., Watkins et al., 2023), and natural gas storage (e.g., Cesca et al., 2021). In a handful of cases, induced earthquakes have led to sufficiently strong ground motions to cause damage to nearby buildings and infrastructure (e.g., Lee et al., 2019; Lei et al., 2019; Campbell et al., 2020). Where induced earthquakes are large enough to be felt, they become a source of significant public concern even if magnitudes are not large enough to cause damage (Evensen et al., 2022). The occurrence of induced seismicity has seen regulators respond by imposing strict regulatory measures; sometimes closing culpable projects, such as gas production at Groningen in the Netherlands (van de Graaff et al., 2018), geothermal energy projects at Basel in Switzerland and Pohang in South Korea (Häring et al., 2008; Lee et al., 2019), and natural gas storage at the Castor site, Spain (Cesca et al., 2021); or imposing significant limitations on injection rates, such as for wastewater disposal in Oklahoma (OCC, 2016). In the UK, a nationwide moratorium on shale gas extraction was imposed because of the perceived inability to manage injection-induced seismicity (BEIS, 2019).

Induced seismicity has been observed at CCS sites (Verdon et al., 2011; 2013; Stork et al., 2015; Dando et al., 2021; Goertz-Allmann et al., 2024), although to date the magnitudes have been small. Nevertheless, these instances demonstrate the importance of managing induced seismicity during CCS operations as the industry grows. Shutdown of CCS projects due to the occurrence of larger magnitude induced events, as has happened in other industries, would have a significant impact on the growth of this nascent technology.

In the UK, the focus of CCS-related activities has been offshore in the North Sea, Irish Sea, and English Channel. The UK government (via the relevant regulator, the North Sea Transition Authority, NSTA) has so far issued 28 licenses for "carbon dioxide appraisal and storage" (we refer to these as "CCS Licenses" hereafter) in these areas (Figure 1). Operational injection of CO_2 at some of these licensed sites is expected to begin by the late 2020s.

The siting of CCS operations offshore can significantly reduce the risks posed by induced seismicity by reducing the exposed population. However, earthquakes induced offshore can still be felt onshore. Induced seismicity at the Castor natural gas storage project provides an important case study in this regard (Cesca et al., 2021): even though the injection site was over 20 km offshore the induced events, which exceeded magnitude M 4.0, were felt by the local population onshore from the site, leading to local opposition and the shutdown of the project. Past tectonic earthquakes in the seas around the UK have been widely felt – the largest tectonic earthquake to have occurred in the UK, the 1931 M 6.1 Dogger Bank event, was in the southern North Sea near to the location of several CCS license blocks (Musson, 2007). The 5.7–5.8 M_L 1580 Dover Straits earthquake, which occurred 15 – 20 km offshore (although its exact location highly uncertain), is considered one of the most damaging earthquakes to have hit the UK, with two deaths in England and several others reported in France and Belgium.

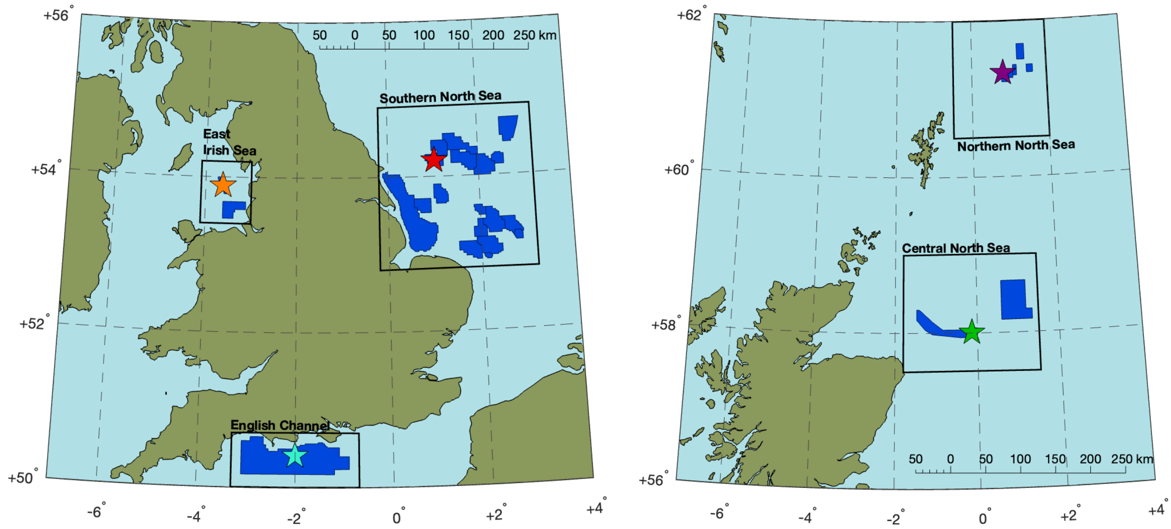

Figure 1: Map of CCS licenses (blue) released by the North Sea Transition Authority in the waters around the UK. The black boxes show our five study regions, and the coloured stars show specific study locations at which risk curves are computed. For ease of visualisation, we split our map into northern and southern portions.

1.1 Management of Induced Seismicity Hazard

Induced seismicity can be managed prior to operations during site selection, and during operations by real time monitoring and decision-making (e.g., Verdon and Bommer, 2021; Schultz et al., 2024a).

The occurrence of induced seismicity requires the presence of critically stressed tectonic faults. The likelihood of induced seismicity will therefore be increased by an greater abundance of faulting (e.g., Schultz et al., 2016; Wozniakowska and Eaton, 2020; Rodríguez-Pradilla and Verdon, 2024), by elevated pore pressures (e.g., Eaton and Schultz, 2018), and by elevated stress conditions (e.g., Verdon and Rodríguez-Pradilla, 2023). These criteria can be used to screen potential targets during the site selection and characterisation phase. However, in practice *a priori* mitigation of induced seismicity in this way is often unsuccessful. In particular, the identification of potentially seismogenic faults during site characterisation can be challenging. Faults of sufficient size to host M 4.0 earthquakes (i.e., roughly km length scale) may only have a displacement of tens of metres, putting them at the limits of resolution for typical reflection seismic surveys (Nantanoi et al., 2022; Rodríguez-Pradilla and Verdon, 2024). Strike-slip faults, which do not produce vertical offset, can be even harder to identify using geophysical methods. Furthermore, the stress perturbations that generate induced seismicity can propagate downwards to reactivate faults in basement strata that are often not investigated in detail during site characterisation. As such, numerous cases exist where faults that hosted induced seismicity were not identified during site characterisation (e.g., Eaton et al., 2018; Cesca et al., 2021; Nantanoi et al., 2022).

Instead, induced seismicity is typically managed by real-time decision-making during operations. Monitoring systems are installed to detect and characterise induced seismic events and this information is used to evaluate the upcoming seismic hazard and to adjust the planned injection program accordingly. In the simplest form, this approach takes the form of a Traffic Light System (TLS), where pre-set magnitude thresholds are defined, typically an “amber light” at which injection rates are reduced and a “red light” at which injection is stopped (Bommer et al., 2006). TLSs are inherently retroactive (decisions are taken in response to observed events), so considerable thought must be given to setting the amber and red thresholds (M_{AMB} and M_{RED}) relative to the actual risk-related objective (e.g., Schultz et al., 2020b; Verdon and Bommer, 2021). TLSs are the most widely used regulatory approach to the management of induced seismicity (Kendall et al., 2019).

As induced seismicity forecasting models have improved, alternative methods, often referred to as Adaptive Traffic Light Systems (ATLSs, Mignan et al., 2017), have been proposed. In this approach, the observed seismicity is used to populate a statistical model that forecasts the upcoming seismicity. The two most common modelling strategies for this purpose are either (i) based on assumptions of linear scaling between injection rates and seismicity rates (e.g., Shapiro et al., 2010; Hallo et al., 2014; Langenbruch et al., 2018; Mancini et al., 2021; Verdon et al., 2024), or (ii) using extreme value theory (e.g., Cao et al., 2021; Watkins et al., 2023; Verdon and Eisner, 2024; Schultz et al., 2024b).

In an ATLS, operations can be amended or stopped if the likelihood of an event of unacceptable magnitude, as estimated by the forecasting model, exceeds a given threshold. This type of approach has now been applied to guide live decision-making at several active injection sites (e.g., Verdon, 2016; Clarke et al., 2019; Kwiatek et al., 2019; Kettlety et al., 2021).

1.2 Tolerable Magnitudes

What these methods share is the need to establish an acceptable level of risk. This is achieved by defining a maximum tolerable magnitude. This point represents the level at which the impact of induced seismicity, defined by either the nuisance of felt events experienced by the public, or the damage to buildings and infrastructure, becomes intolerable. We refer to this tolerable magnitude as M_{TOL} hereafter. For TLSs, M_{RED} must be set an appropriate level below M_{TOL} to ensure that magnitude jumps and/or trailing seismicity (continued induced earthquakes that occur after injection has stopped) do not exceed M_{TOL} (e.g., Schultz et al., 2020b; Verdon and Bommer, 2021; Zhou et al., 2024). For ATLSs, M_{TOL} must be defined such that operations are stopped or amended if forecasting models indicate that this threshold is likely to be breached.

We note that M_{TOL} is determined by the ground motions produced by a given event as experienced by local populations and infrastructure. The ground motions will depend on the earthquake hypocentre, the local ground characteristics, and the distance to the exposed population. However, these factors are typically relatively constant for a given injection site: induced earthquake hypocentres will be located within the region that is perturbed by the injection; the local ground characteristics will not change over the typical durations of interest; and nor will the locations of exposed populations. As such, M_{TOL} can typically be defined for a given injection site based on considerations of expected ground motions for a given magnitude event at the injection site, as felt by nearby populations.

M_{TOL} will also depend on willingness of a local population to tolerate induced seismicity, and on the vulnerability of exposed buildings. Public communication campaigns undertaken prior to the onset of operations can help the public to understand and expect induced seismicity, which can improve public willingness to tolerate it. In extreme cases, Bommer et al. (2015) proposed that structural upgrading of vulnerable buildings could be a more appropriate way of managing induced seismicity risks that cannot otherwise be avoided.

Schultz et al. (2023) developed a method to characterise tolerable magnitudes for induced seismicity specifically within the context of UK shale gas development. They estimated the tolerance of the public for given impacts (e.g., nuisance and damage) based on the impacts generated by observed events, and the public and regulatory response thereto. Given the current situation with respect to CCS developments around the UK (and given that the moratorium on shale gas development in the UK remains in place), there is a clear need to reprise this analysis for the CCS license blocks that have been awarded by the NSTA.

In estimating tolerable levels of induced seismicity for UK shale gas operations, Schultz et al. (2023) went one step further. Since the regulator had applied TLS regulations to shale gas activities in the UK, Schultz et al. (2023) sought to estimate appropriate TLS M_{RED} thresholds based on assumptions about magnitude jumps and trailing seismicity. In contrast, the relevant regulatory bodies have not specified how they intend to manage induced seismicity risks during CCS development in the UK. Our preference in this study is therefore to estimate M_{TOL}, the magnitude threshold at which we anticipate that the impacts of induced seismicity from CCS would become intolerable to the public, thereby leaving open the question of how best to ensure that these levels are not exceeded.

We note that in estimating M_{TOL} based on the response of the public to nuisance and/or damage, we do not consider the potential impacts of induced seismicity on offshore infrastructure, which will consist of the pipelines, platforms and wells of the CO_2 injection facilities themselves, and may also include offshore hydrocarbon pipelines, wells and platforms (some of which may have been decommissioned), and offshore wind farms. Separate induced seismicity risk assessments may be required for such structures. Also, we do not consider the potential geomechanical hazards posed by induced seismicity, such as deformation of wellbores due to fault slip, or the creation of permeable leakage pathways through sealing caprocks (e.g., Verdon et al., 2013).

2. METHOD

Our approach is based on the methods developed by Schultz et al. (2021a; 2021b; 2023). We briefly recap the approach here. Since we are only interested in defining M_{TOL} in this study, we do not incorporate trailing seismicity effects. The Schultz et al. (2023) approach is based on a Monte Carlo analysis of the impacts of induced seismicity occurring at a given location. Ground motions are simulated for a given earthquake position and magnitude. Nuisance and fragility functions are then used to estimate the likelihood of experiencing different levels of nuisance and damage states. These likelihoods are then used to estimate the numbers of households that would experience a given impact, based on population density maps.

Schultz et al. (2023) evaluated the tolerability of a given level of impact based on the impacts of previous induced seismic events in the UK. Based on estimated levels of nuisance and damage for past acceptable and non-acceptable induced events, Schultz et al. (2023) were able to infer acceptable tolerances for different levels of nuisance and damage in terms of the aggregate numbers of households affected.

2.1. Ground Motions and Impacts

For a given earthquake hypocentre and magnitude, we compute peak ground velocities (PGV) using the Edwards et al. (2021) ground motion model (GMM). This GMM was developed specifically for induced seismicity at UK shale gas sites. In order to account for analastic attenuation due to the longer distances involved in the CCS cases considered here, we implement the additional distance scaling term (-0.0006R) recommended by Atkinson (2015). In implementation for our target sites, site amplification effects were estimated using a global slope-based proxy for V_{S30} (Heath et al., 2020), shown in Figure 2. In our Monte Carlo analysis (see below), V_{S30} values are perturbed by their standard errors, and ground motions outputs are perturbed according to their inter-event standard deviation. Ground motions are further perturbed by a spatially correlated intra-event error calibrated for European data (Esposito and Iervolino, 2012; Edwards et al., 2021).

We translate modelled ground motions into probabilities of experiencing different impacts based on nuisance/fragility functions. We categorise the degree of nuisance by Community Decimal Intensity (CDI, Wald et al., 2012), where levels CDI-2 – CDI-6 correspond to “just felt”, “exciting”, “somewhat frightening", "frightening", and "extremely frightening". We use the nuisance function developed by Schultz et al. (2021c) to estimate the likelihood of experiencing these CDI levels as a function of PGV. At low PGV values (< 0.1 mm/s) the shape of the respective nuisance curves estimated by Schultz et al. (2021c) creates the implausible outcome that the likelihood of experiencing higher CDI levels (CDI-3 – CDI-6) becomes higher than that of lower CDI levels (CDI-2). This issue had an insignificant impact when applied by Schultz et al. (2023) to shale gas induced seismicity where large populations were found relatively close to the proposed sites. However, for offshore CCS sites this becomes an issue because populations are all relatively far from the modelled hypocentres, and so all receive low ground-motions for moderate magnitude events, creating the outcome that the risk curves for higher CDI levels can be above those for lower CDI levels. We correct this by setting the likelihoods for nuisance to zero below a PGV of 0.1 mm/s. Note that British Standards BS 5228 (BSI, 2014) gives the threshold for perception of vibrations at 0.14 – 0.3 mm/s.

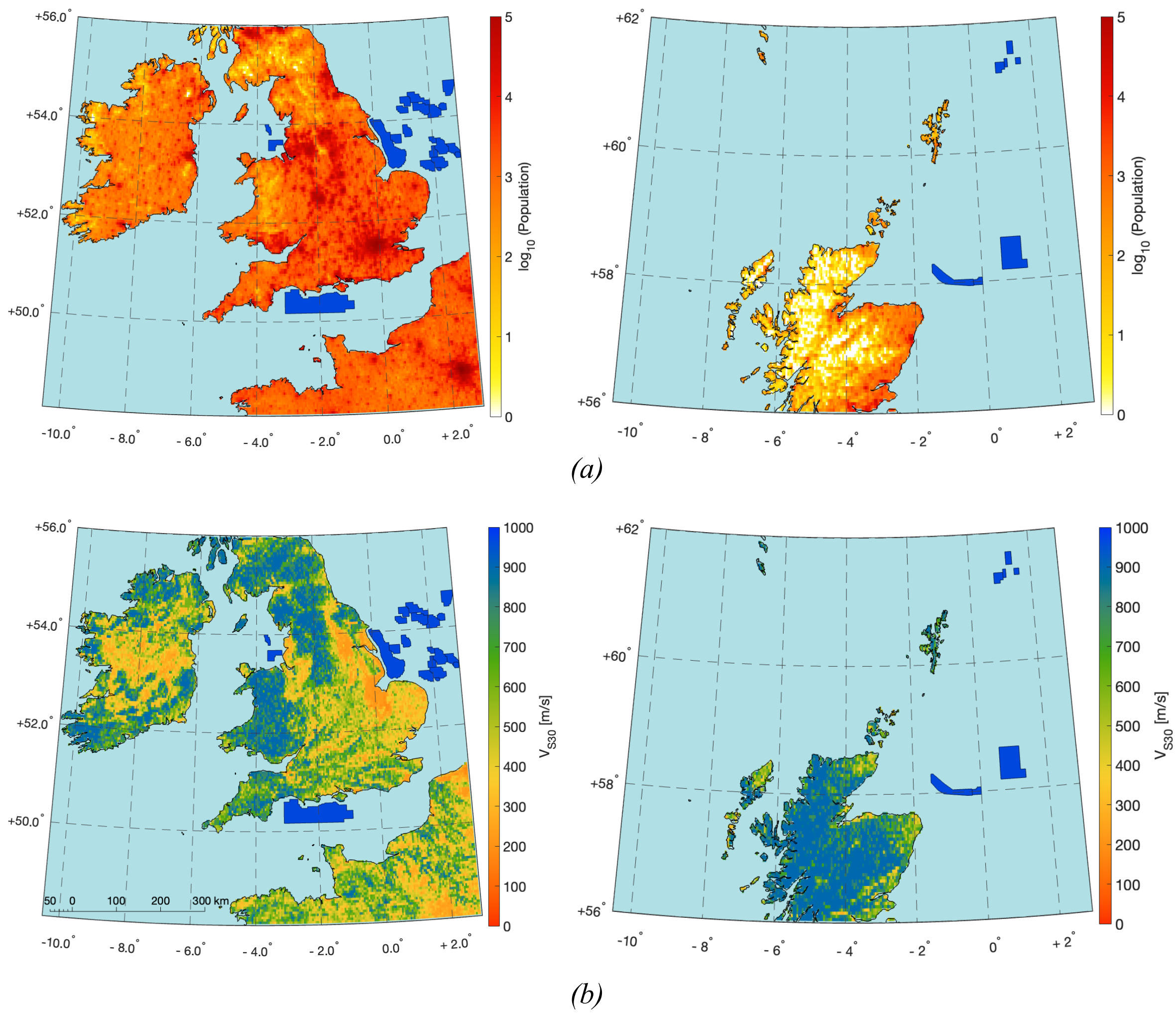

Figure 2: Maps of UK population (a) and V_{S30} based on slope proxy (b). CCS licenses are shown in blue. For ease of visualisation, we split each map into northern and southern portions

We use the fragility function computed for induced seismicity at Groningen in the Netherlands (Korswagen et al., 2019) to compute the likelihood of damage for a given PGV value. The likelihood of damage is estimated at two states, DS-1, which corresponds to visible light damage (> 0.1 mm cracks) and DS-2, which represents easily observable light damage (> 1 mm cracks). We set the likelihoods for damage to zero below a PGV of 0.5 mm/s. British Standards BS 5228 (BSI, 2014) gives a lowermost threshold for cosmetic damage in unreinforced or light framed structures at 15 mm/s. The damage function includes a pre-damage term Ψ_0 (Korswagen et al., 2019), which we sample from a half-Gaussian distribution. Uncertainties in nuisance and damage functions were considered through perturbations of their input parameters in our Monte Carlo analysis.

Schultz et al. (2023) also computed a third risk metric, the local personal risk (LPR) that computes the likelihood of suffering a fatality due to building collapse, which can provide a useful comparison with other risks. However, they found that the tolerable levels for nuisance and cosmetic damage (CDI-2 – CDI-4 and DS-1 – DS-2) were reached at much lower magnitudes than the LPR threshold, and so LPR did not define acceptable magnitudes for induced seismicity. As such, we do not calculate LPR in this study.

The severity of risk, in terms of the numbers of households affected at a given nuisance or damage level, is then estimated by multiplying the impact likelihood by the number of households at the given grid point. Our populations (shown in Figure 2) are taken from the LandScan model (Rose et al., 2019) and we assume, based on UK census data, an average of 2.4 residents per household to estimate the numbers of households. The total numbers of households affected is then calculated by summing the numbers from each grid point.

We adopt the criteria used by Schultz et al. (2023) to define the levels of tolerable impacts. Schultz et al. (2023) reached these criteria by examining the impacts from induced earthquakes in the UK. Specifically, they studied the Preese Hall (Clarke et al., 2014), Preston New Road PNR-1z (Clarke et al., 2019) and Preston New Road PNR-2 (Kettlety et al., 2021) hydraulic fracturing-induced sequences in Lancashire, and the Newdigate sequence in Surrey (Hicks et al., 2019), which were actually natural earthquakes but nevertheless triggered a response from the regulator given their proximity to oilfield operations. Schultz et al. (2023) computed the expected impact from each event in terms of nuisance and damage using the modelling approach outlined above and assessed whether each of the events in question were tolerated by nearby populations based on public and regulatory responses to each event. By doing so, they were able to identify tolerances for each nuisance and damage criterion that seemed to delimit acceptable versus unacceptable events.

From Schultz et al. (2023), the estimated tolerance of nuisance was reached when the median expected numbers of affected households reached 9,571 for CDI-2, 5,478 for CDI-3, and 2,719 for CDI-4. The estimated tolerance of damage was reached when the median expected numbers of affected households reached 0.1 for DS-1 and 0.0001 for DS-2. The values for DS-1 and DS-2 being below 1 imply a 1-in-10 and 1-in-10,000 chance of a household experiencing damage at these levels. The fact that the Schultz et al. (2023) damage tolerances are less than 1 indicates that the public tolerance for induced seismicity is such that earthquakes can be intolerable where damage, even of a cosmetic nature, is unlikely to occur – nuisance alone can be sufficient to render a given level of induced seismicity impact intolerable in the eyes of the public.

It is nevertheless of interest to examine magnitudes at which observed levels of damage (of a minor and cosmetic nature) might begin to be observed. We therefore also compute an additional tolerance, where the number of affected households exceeds 10 for DS-1. We refer to this tolerance as [$N(DS\text{-}1) \geq 10$] hereafter. As well as being of interest to operators of CCS sites as a magnitude at which damage becomes likely (as opposed to the DS-1 and DS-2 criteria above, where the likelihood of damage is still low, though not impossible), this threshold will also be relevant when comparing our tolerance estimates with the observations of damage (or the lack thereof) from past natural earthquakes located in the seas around the UK (see Section 4.2).

2.2. Monte Carlo Sampling

We use a Monte Carlo approach to sample the uncertainties in each of our input parameters. Within each of our study areas (English Channel; East Irish Sea; southern North Sea; central North Sea;

northern North Sea; as shown in Figure 1), we sample potential induced earthquake source locations on "source grids" of 0.025° Latitude × 0.05° Longitude (roughly 2.5 × 2.5 km) across five regions of interest: English Channel, East Irish Sea, southern North Sea, central North Sea, and northern North Sea (Figure 1). For each potential source location, we simulate earthquakes across a range of magnitudes from $1.0 \leq M \leq 6.5$, at 0.1 unit increments. We set our upper limit at M 6.5 as this value has been used to represent M_{MAX} (i.e., the maximum possible earthquake magnitude) for induced seismicity in the UK by Mancini et al. (2021), who adopted this value as it lies at the lower end of the range of values estimated for tectonic earthquakes. In curtailing our hazard calculations at this limit, we make no judgement as to where this value really does represent M_{MAX} for induced seismicity in the UK, since there are sound reasons why tectonic M_{MAX} values should not be adopted uncritically for induced seismicity cases (Bommer and Verdon, 2024).

For each source position and magnitude, we perform 1,000 iterations with random perturbations to each input parameter. For each modelled earthquake, we compute the shaking and the resulting impacts across a "shake grid" with increments of 0.05° × 0.05° (Lat/Lon) that covers the entirety of the United Kingdom, plus Ireland and northern France (Figure 2).

CCS operations that seek to inject CO_2 as a supercritical fluid will target reservoirs that are deeper than 700 – 800 m, though some projects may inject CO_2 in the gas phase at shallower depths. Observations show that induced earthquakes often occur in the crystalline basement underlying injection targets in sedimentary rocks (e.g., Verdon, 2014). We therefore sample earthquake depths across a uniform distribution from 1 – 5 km depth. Given the larger epicentral distances from the offshore CCS licenses to the nearest population centres, earthquake depth has a minor impact on our results, in contrast to the shale gas sites considered by Schultz et al. (2023), many of which were very close to population centres. The perturbations that we apply to each of the parameters that determine the ground motions and resulting impacts are shown in Figure 3.

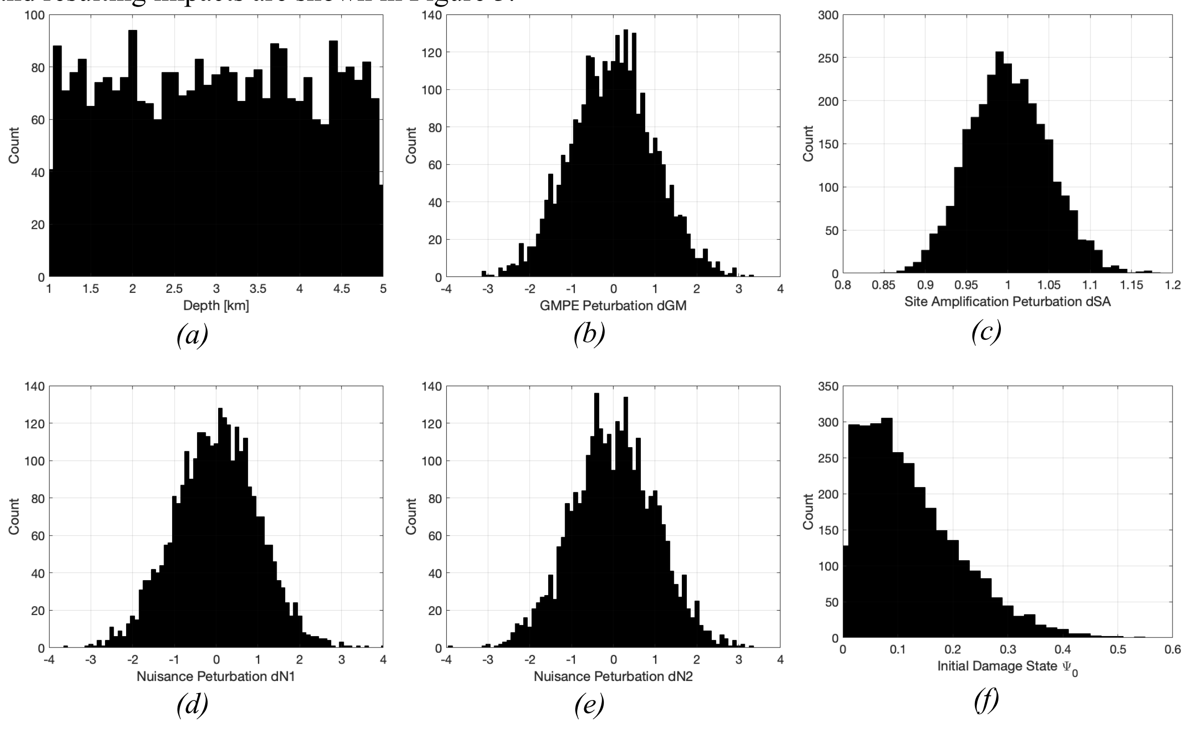

Figure 3: Perturbations applied to input variables for our Monte Carlo analysis.

For each point in the source grid, the outcome is a risk curve that shows the numbers of households that would experience different impacts from induced earthquakes of different magnitudes. Example curves for four selected sites are plotted in Figure 5. We define M_{TOL} at that source point as the magnitude at which the median number of impacted households exceeds the tolerance for the given impact metric, as defined above.

3. Results

In Figure 4 we plot risk curves for five representative sites: Endurance (southern North Sea), Morecambe (East Irish Sea), English Channel, Goldeneye (central North Sea), and Tern (northern North Sea). The locations of these sites are plotted in Figure 1. As might be anticipated, the resulting outcomes are strongly dependent on the positions of these sites relative to the coast. The English Channel and Morecambe sites are both within 30 km of the coast, and near to relatively dense population centres. As a result, the risk curves are higher. The Endurance site is approximately 65 km from the shore, and the resulting curve is lower. The Goldeneye site is over 80 km from the shore, and that shoreline is sparsely populated in northeast Scotland, while the Tern field is over 100 km from the Shetland Islands, and over 350 km from the Scottish mainland. As a result, the risk curves for these sites are significantly lower.

Comparing the risk curves in Figure 4 with those plotted in Schultz et al. (2023) (Figure 4 of that paper), we see that our curves are generally steeper at lower magnitude values, with gradients decreasing as magnitudes increase. In contrast, the curves generated by Schultz et al. (2023) are more linear across the M vs. log[No. of households] space. This reflects the more binary nature of impacts for the offshore sites modelled in our study, where if the ground motions are not large enough to be felt onshore, then obviously they will impact nobody, but if they are large enough to have impact onshore then those impacts could be felt by large numbers of people all along the shoreline. This contrasts with the situation for onshore activities, where the numbers of people impacted will increase relatively linearly with distance from the site in question.

In Figures 5 – 7 we map M_{TOL} values for nuisance and damage for each of the 5 study areas. Specifically, we use the CDI-3, DS-1 and DS-2 tolerances defined by Schultz et al. (2023). The M_{TOL} values for CDI-2 and CDI-4 are very similar to those for CDI-3 (see Supplementary Materials). We find that M_{TOL} values for DS-1 are generally slightly higher than for CDI-3, typically by around 0.25 magnitude units, while the M_{TOL} values for DS-2 are significantly higher than for CDI-3, by around 1.5 magnitude units.

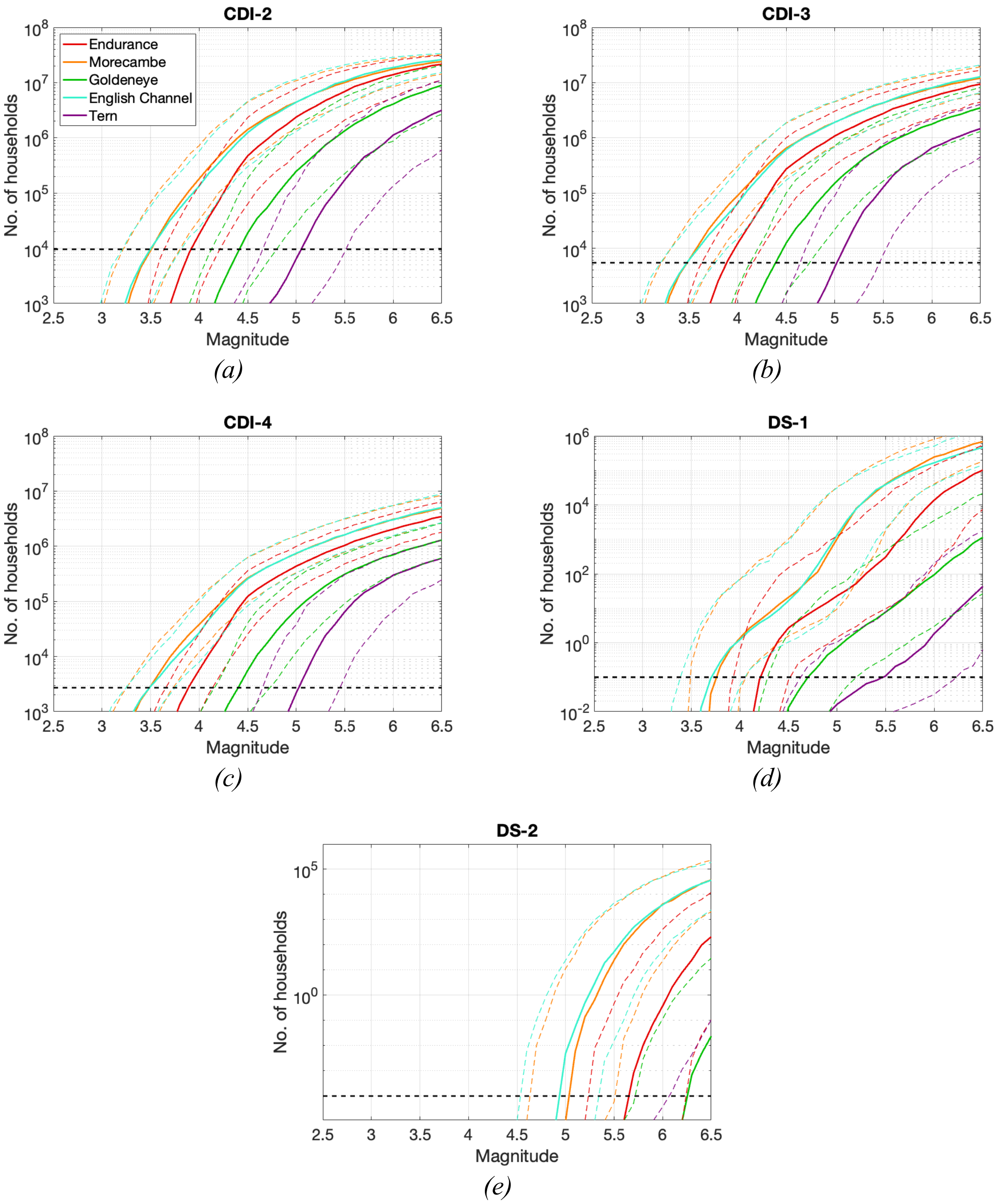

Figure 4: Risk curves for five potential CCS sites around the UK, showing the numbers of households expected to experience a given impact (CDI-2 to CDI-4 (a – c), DS-1 (d), and DS-2 (e)) as a function of magnitude. Solid lines show median values from our Monte Carlo analysis, dashed lines show 5 % and 95 % upper and lower values. The curve colours correspond to the five positions mapped as coloured stars in Figure 1: turquoise = English Channel; orange = Morecambe gas field, East Irish Sea; red = Endurance, southern North Sea, green = Goldeneye, central North Sea, purple = Tern site, northern North Sea. Note that no DS-2 impacts are reached for the Tern site within our magnitude range. Horizontal black dashed lines show risk tolerances defined by Schultz et al. (2023).

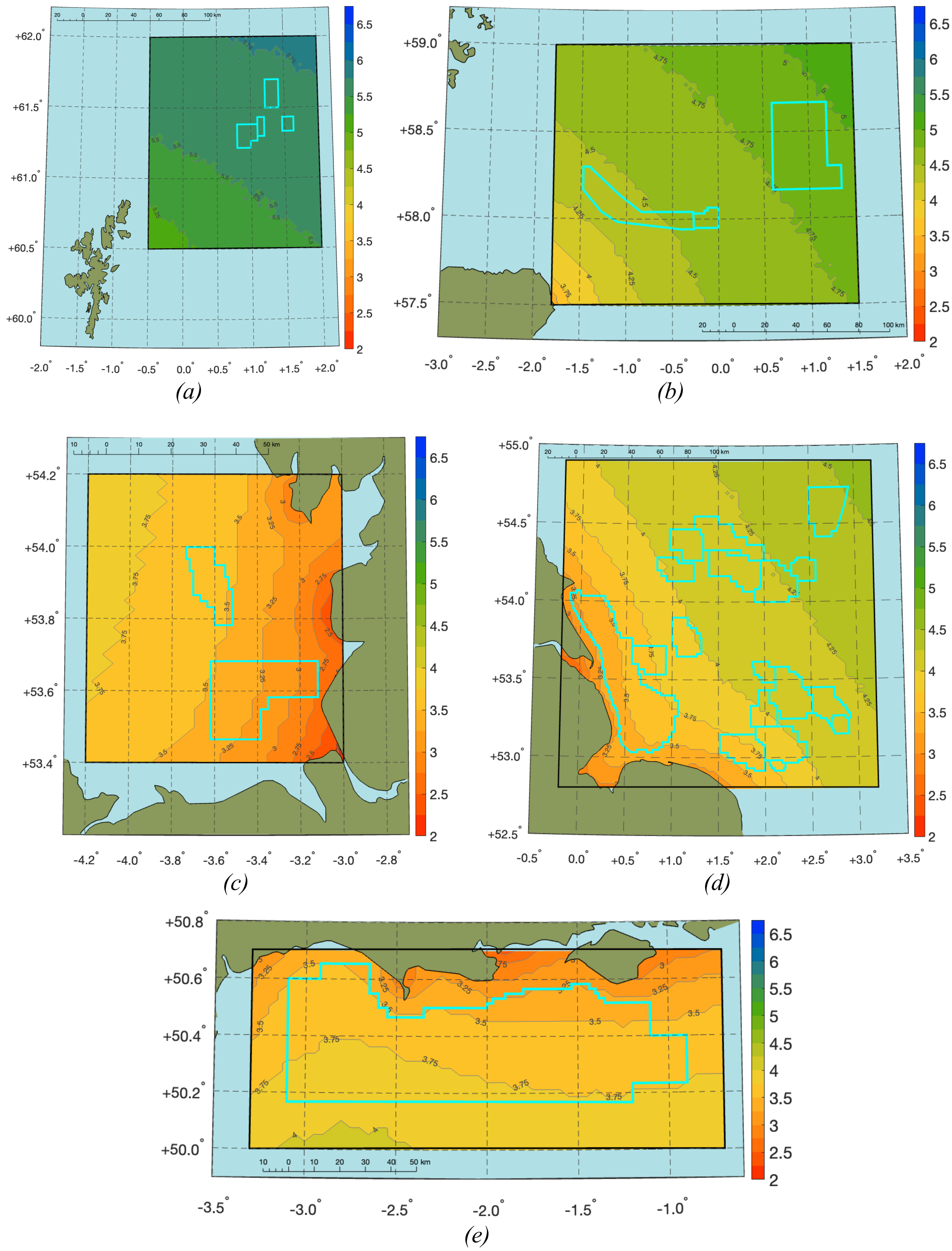

Figure 5: Maps of M_{TOL} values based on nuisance impacts (CDI-3) for each of our 5 study areas: northern North Sea (a), central North Sea (b), East Irish Sea (c), southern North Sea (d), and English Channel (e). CCS license blocks are outlined in light blue, and the full study areas are outlined in black.

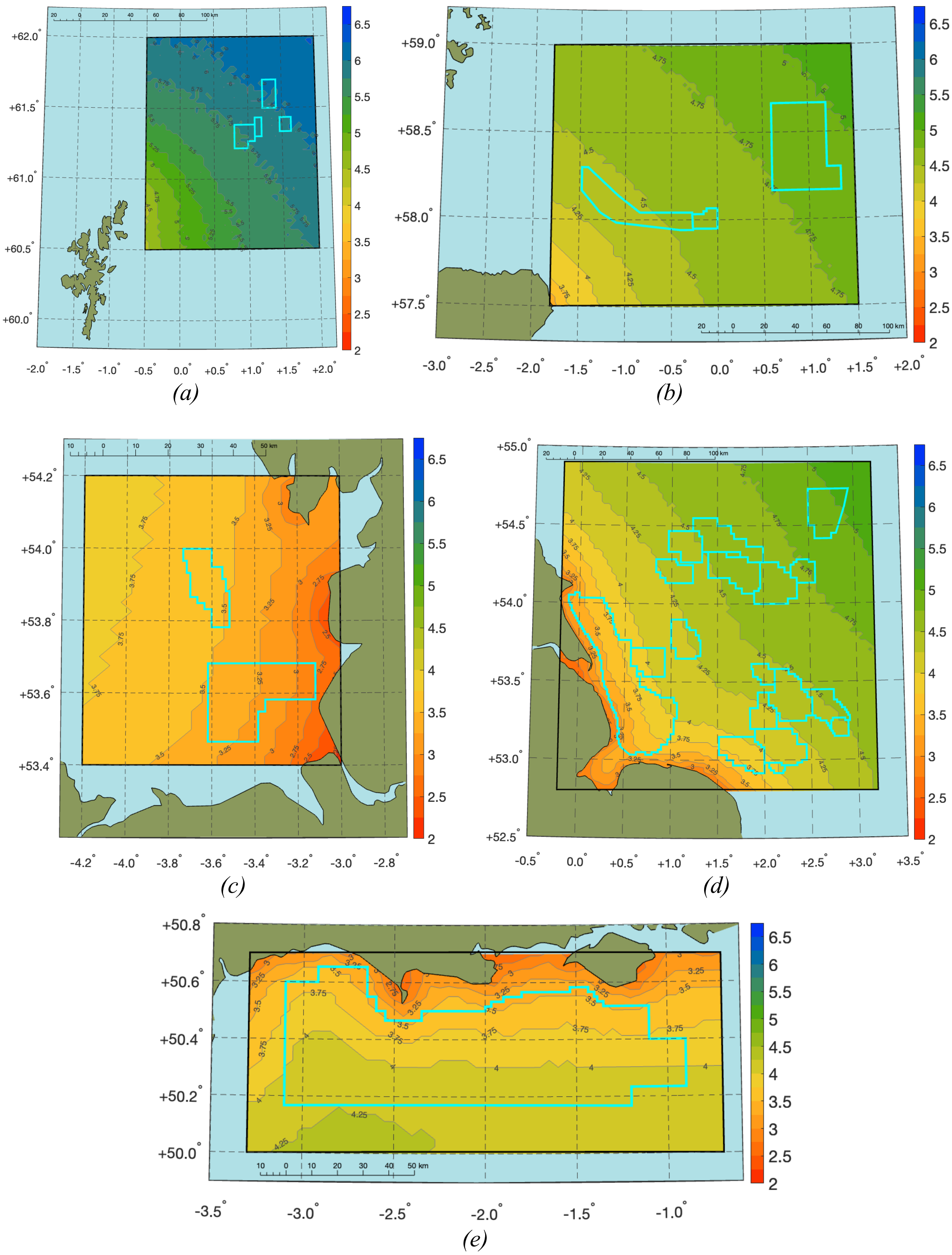

Figure 6: Maps of M_{TOL} values based on damage impacts (DS-1) for each of our 5 study areas. Figure format as per Figure 5.

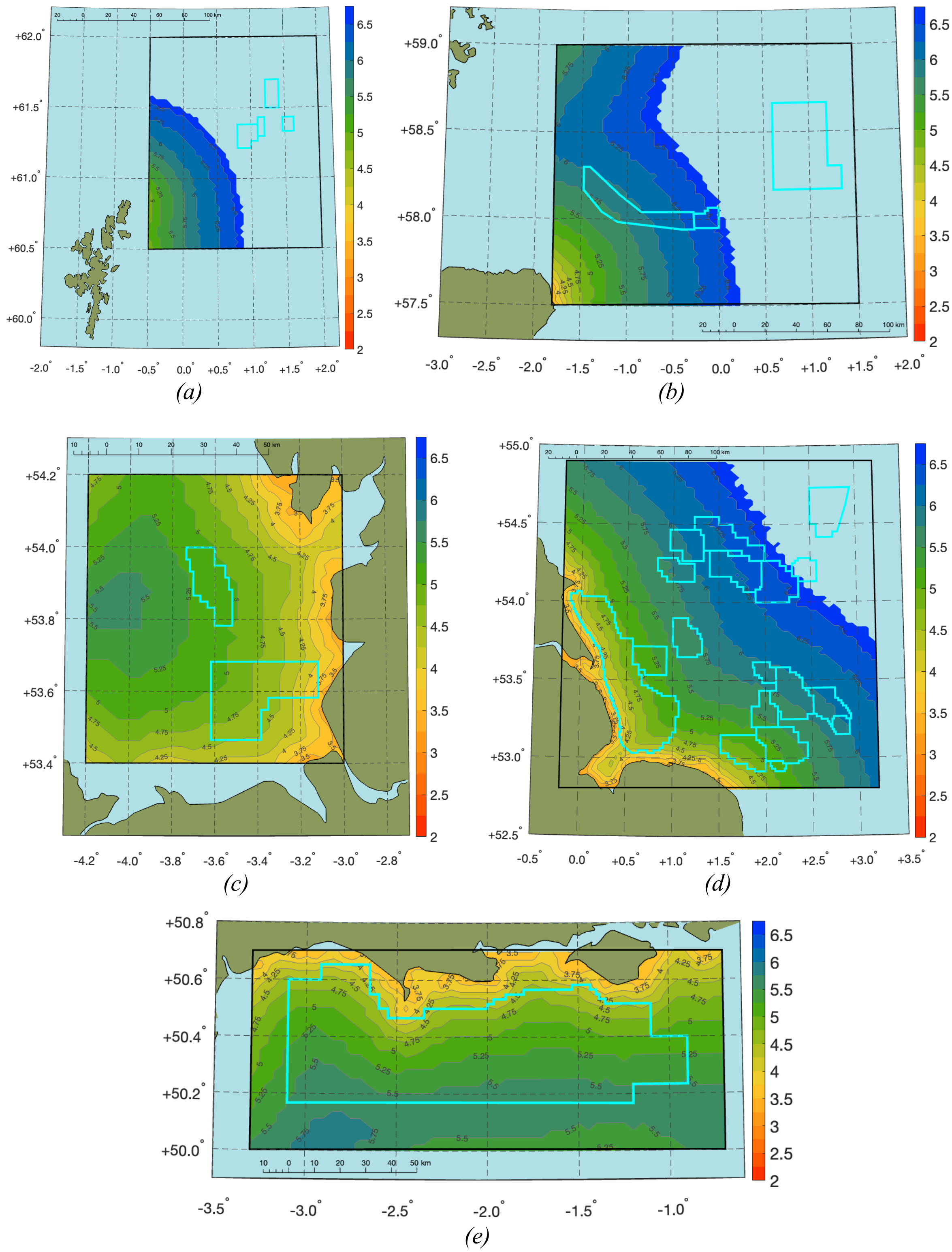

Figure 7: Maps of M_{TOL} values based on damage impacts (DS-2) for each of our 5 study areas. Figure format as per Figure 5. M_{TOL} values are left blank where magnitudes of M 6.5 did not exceed the risk tolerances.

Our criterion whereby cosmetic damage might be expected to be observed, [*N*(DS-1) ≥ 10], is shown in Figure 8. This tolerance is generally around 1 to 1.5 magnitude units higher than the CDI-3 nuisance tolerance.

4. DISCUSSION

4.1 M_{TOL} as a function of distance to shore

Inspection of Figures 5 – 8 shows that the main control on M_{TOL} values is the distance from the coastline. This is to be expected, because the distance from shore represents the minimum distance to the nearest populations that could experience nuisance or damage, and therefore controls the ground motions that are experienced for a given magnitude. To further investigate this, in Figure 9 we plot the M_{TOL} values for nuisance and damage (CDI-3 and [N(DS-1) $\geq$ 10]) for every grid point in our study areas, as a function of the distance to the nearest point on the coast. We find that the M_{TOL} values for the southern North Sea, East Irish Sea and English Channel fall along very similar trends. The M_{TOL} values for the central and northern North Sea areas are substantially higher for a given distance to shore, with the central North Sea typically being roughly 0.5 units higher at a given distance, and the northern North Sea being roughly 1.0 units higher. This may reflect the fact that the shorelines facing the central and northern North Sea areas are substantially less populated than those facing the East Irish Sea, southern North Sea and English Channel.

For the northern North Sea, the nearest coastline is the Shetland Islands, which has a total population of roughly 20,000 people. Since we assume 2.4 people per household, this amounts to only 8,333 households, so nearly every household would need to experience nuisance at CDI-3 to reach the Schultz et al. (2023) tolerance. It might be argued that the Schultz et al. (2023) tolerances, calibrated via experiences of induced seismicity in medium-sized English towns such as Blackpool and Crawley, will not be appropriate for a small and isolated community such as the Shetland Islands, leading to an overestimation of M_{TOL}. Additionally, consideration of local risk metrics for nuisance (rather than only aggregate) could be incorporated into future work, to ensure that an individual's chance of experiencing nuisance is accommodated as well.

In Figures 9b and 9d, we show M_{TOL} as a function of the distance to the nearest population grid that has a population of at least 10,000 people. This normalises the behaviour between the different study areas to a degree. However, the M_{TOL} values for the central and northern North Sea areas are still slightly higher at a given distance. This may reflect the fact the V_{S30} values for northern Scotland are generally higher than England (Figure 2), resulting in lower amplification effects, and the fact that, while there are high density population centres in northeastern Scotland (most notably Aberdeen and Inverness), the general density of population is significantly lower.

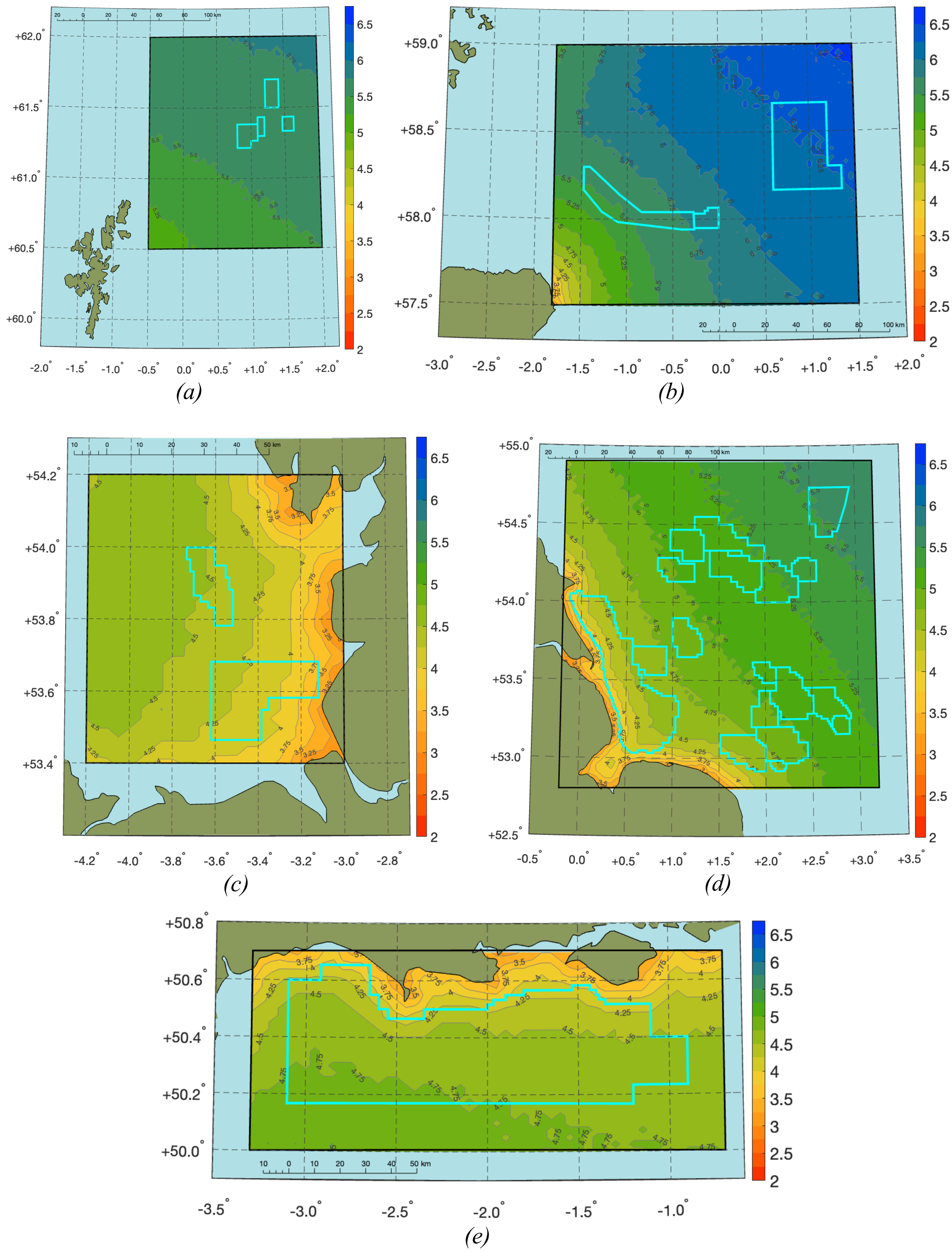

Figure 8: Maps of M_{TOL} values based on a tolerance where minor damage might be expected (N(DS-1) = 10), for each of our 5 study areas. Figure format as per Figure 5. M_{TOL} values are left blank where magnitudes of M 6.5 did not exceed the risk tolerances.

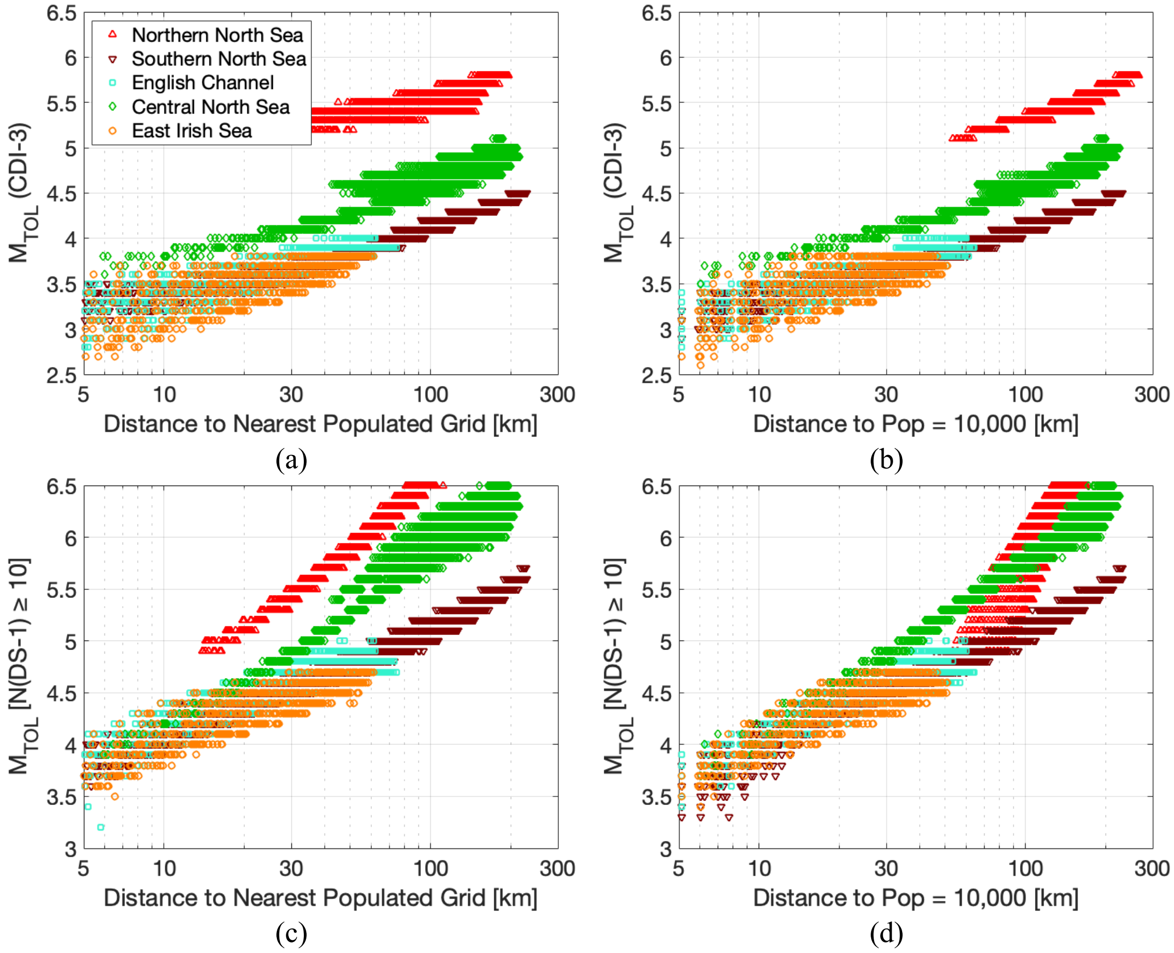

Figure 9: M_{TOL} as a function of distance. In (a) we show M_{TOL} values for nuisance (CDI-3) for each of our study areas as a function of distance from the nearest coastline. In (b) we show the same as a function of distance from the nearest densely populated area (with a population > 10,000). In (c) and (d) we show the same for M_{TOL} values for damage [N(DS-1) ≥ 10].

4.2 Comparisons with past UK earthquakes

We can use the observed macroseismic impacts of past earthquakes around the UK in order to sense-check the M_{TOL} thresholds estimated above. Specifically, we examine the observed macroseismic impacts for past events and assess whether they are consistent with such events being tolerable if they had been induced events. Clearly this is a subjective judgement, as we cannot know whether these historical events, had they been induced by industrial activities, would have actually been tolerated or not. However, it is reasonable to assume that events that were strongly felt across widespread areas would be unlikely to be tolerable were they induced. Events that were mildly felt by small numbers of people in localised areas would be more likely to be tolerable. Offshore events that were not felt onshore would be tolerable. We compare the observed impacts with our M_{TOL} values for nuisance (CDI-3), and with our M_{TOL} values for damage at [*N(DS-1)* ≥ *10*].

It should be noted that the population densities at the time for historical events were significantly lower, which could serve to reduce the overall impact relative to our models (which use modern population densities), and that the following events are all natural earthquakes, most of which are located at greater depths than would be expected for induced earthquakes.

An exact match between observed impacts and our risk estimates should not be expected, given the above differences, as well as the inherent variability in earthquake ground motions and impacts. The risk curves plotted in Figure 4 give an indication of this variability: the risk curves at 5 % and 95 % are typically around 0.50 – 0.75 magnitude units above and below the median values. Nevertheless, the observed impacts from these events can provide a useful guide as to whether our M_{TOL} estimates are realistic. Figure 10 shows a map of historical and instrumentally recorded earthquakes around the UK, with the specific earthquakes discussed below highlighted. We examine each CCS license area in turn.

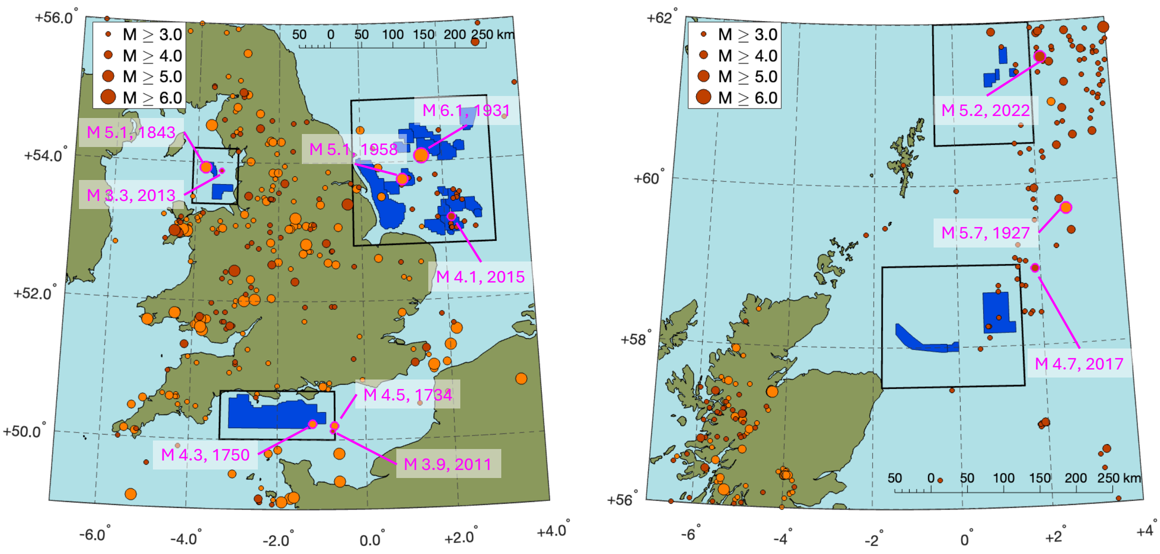

(a) *(b)*

Figure 10: Map of historically identified (orange circles) and instrumentally recorded (red circles) earthquakes with $M \geq 3.0$ across the southern (a) and northern (b) UK. Events are sized by magnitude. Earthquakes discussed specifically in Section 4.1 are outlined in pink and labelled.

Southern North Sea

The largest earthquake in the UK for which a reliable magnitude has been estimated is the July 1931 M 6.1 Dogger Bank event in the southern North Sea (Versey, 1939). The estimated location for this event is quite close to several CCS license blocks. The event was felt across the whole of the UK, as well as parts of Ireland, northern France, Belgium, the Netherlands, Denmark and southern Norway. Minor damage occurred along the east coast of England (Musson, 2007), with cases of chimneys and plaster being damaged. The most notable example of damage was to the spire of the Wesleyan Chapel in Filey, which was rotated by 2 inches (Sargeant and Musson, 2009). However, in no case were the impacts severe enough to be unequivocally judged to be at VII on the Medvedev–Sponheuer–Karnik intensity scale (Neilson et al., 1986). Impacts of this nature would be unacceptable from an induced event from the perspectives of nuisance and damage. Our M_{TOL} value for nuisance at the location of this event is approximately M_{TOL} = 4.1, and our M_{TOL} for damage ([*N(DS-1) = 10*]) is approximately M 5.0. Hence, the fact that this event would likely not be tolerable in terms of nuisance as an induced event, and that it caused observable damage, is consistent with its magnitude exceeding both these values.

The February 1958 M 5.1 event in the southern North Sea was smaller than the Dogger Bank event described above, but it was closer to the coast. This event was felt along the east English coast, as far inland as Nottingham – including by members of the Royal Family at the Sandringham Estate in northern Norfolk (BGS, 2010). However, there was probably no damage from this event (BGS, 2010).

Our M_{TOL} value for nuisance at the location of this event is approximately M 3.8, and M_{TOL} for damage is approximately M 4.9, so our model expectation is that this event would likely not be tolerable from a nuisance perspective, and it could have the potential cause damage. Hence, the fact that the observed impacts from this event would be unlikely to be tolerable in terms of nuisance is consistent with our model. The absence of recorded damage for this event is not consistent with our model estimate but, given the expected variability in outcomes as described above, not to a significant degree.

In August 2015, an M 4.1 event occurred in the southern North Sea, located close to the southernmost CCS license blocks in this area. A few people in Sheringham and Hickling (two small towns in north Norfolk, about 30 km apart) reported feeling "a slight, but noticeable, vibration for a few seconds" (Galloway, 2016). The event was also felt by workers on the Shell Leman Alpha Complex, who reported that they "felt the platform swaying and there was an audible bang" (Galloway, 2016). The event was assigned a macroseismic intensity of III by the British Geological Survey. Given the small number of felt reports, nuisance impacts from this event would likely be acceptable were they to come from an induced event. However, given that people over 30 km apart reported feeling this event, then it could potentially have been felt by many more people. It therefore likely falls at the upper limit of tolerability. Our M_{TOL} value for nuisance at the position of this event is M 3.9, and for damage is M 4.9. Although our nuisance threshold is slightly lower than the magnitude of this event, we do not consider this to be inconsistent given the inherent variability in earthquake ground motions. The absence of damage from this event is consistent with the event magnitude being below our damage threshold.

English Channel

Two earthquakes located in the English Channel to the south of Portsmouth, towards the southeast of the CCS license block in this area, are reported in the BGS historical database (BGS, 2010) – with M 4.5 in October 1734 and with M 4.3 in March 1750. Given the historical nature of these earthquakes, their position and magnitude should be treated as being highly uncertain. Both events were reported as felt across the south coast, from Bridport in Dorset to Brighton, and as far inland as Bath and London (BGS, 2010). No damage is reported in the BGS database associated with these events. However, given the area across which these events were felt, the nuisance impacts would likely be intolerable for an induced event. These impacts are consistent with our M_{TOL} thresholds for the area in question – M_{TOL} for nuisance is approximately M 3.8, while M_{TOL} for damage is approximately M 4.8.

In July 2011, an M 3.9 event was recorded in the English Channel, slightly to the southeast of the CCS license block (Galloway, 2012). This event was felt along a 100 km stretch of the coastline between Portsmouth and Eastbourne (Galloway, 2012). The BGS assigned a macroseismic intensity of III to this event. The fact that this event falls above our M_{TOL} for nuisance but below our M_{TOL} for damage is consistent with the fact that it was widely felt but did not cause any reported damage.

East Irish Sea

The largest historical event in the East Irish Sea was an M 5.1 event in March 1843. The BGS (2010) database reports that this event was felt throughout most of northern England, southern Scotland, northern Wales, and eastern Ireland. Along the northwestern coast of England, the event caused considerable alarm, but no damage (BGS, 2010). Minor amounts of damage were reported on the Isle of Man. Our M_{TOL} threshold for nuisance in this area is M 3.6, and our M_{TOL} for damage is approximately M 4.6. The impacts from this event are consistent with its magnitude being significantly larger than the M_{TOL} values for nuisance, and slightly larger than that for damage.

A magnitude M 3.3 event occurred August 2013 in the East Irish Sea, approximately 25 km from the coast. Felt reports from this event came mostly along a short stretch of coast at the northern end of the

Fylde Peninsula, though single felt reports were also received from the Isle of Man, Anglesey and Liverpool (Galloway, 2014). The felt reports generally indicate fairly mild impacts, though the BGS assigned a macroseismic intensity of III (Galloway, 2014). The M_{TOL} thresholds for nuisance and damage in this area are 3.3 and 4.3, respectively. The impacts from this event are consistent with its magnitude being below our M_{TOL} for damage, and similar to our M_{TOL} for nuisance (given that the event appears to have been somewhat widely felt, albeit not alarmingly so).

Central and Northern North Sea

Our M_{TOL} for damage in these regions generally exceeds the magnitudes of earthquakes that have occurred in the central and northern North Sea, such that we do not expect to have seen damage from such events. Across much of our central and northern North Sea study areas, our tolerance criteria for damage were not reached at our assumed M_{MAX} value for induced seismicity ($M_{MAX} = 6.5$), and so no M_{TOL} values have been estimated.

The 1927 M 5.7 event in the central North Sea was the second-largest British earthquake in the twentieth century (Musson, 2007), after the southern North Sea event described above. It was felt over most of Scotland and along the eastern coast of England. However, it did not cause any reported damage (Musson, 2007). The location of this event lies between our central and northern North Sea study areas. Interpolating between our calculations, the likely M_{TOL} threshold for nuisance in this area is between M 4.5 – 5.0. The nuisance impacts from this event are consistent with its magnitude being above our threshold for nuisance, while the absence of damage is consistent with this event being below our M_{TOL} value for damage (which, as above, has not been estimated as it would exceed M_{MAX}).

The March 2022 M 5.2 event in the northern North Sea lies just to the east of our northern study area. It was felt in Norway, the Shetlands, and the northeast Scottish mainland, and assigned a macroseismic intensity of IV by the BGS (Galloway, 2023). Our M_{TOL} for nuisance in this area around M 5.1, and the felt impacts from this event are consistent with its magnitude being above our M_{TOL} for nuisance.

In June 2017 an M 4.7 event occurred just to the east of our central study area. It was felt in the Shetlands, Orkneys, and in some places along the northeast Scottish mainland (Galloway, 2018). Reports generally describe relatively mild impacts, such as a "rumbling noise", "like a heavy lorry" passing by, or rattling windows and doors (Galloway, 2018). Our M_{TOL} for nuisance in this area around M 4.7, and the impacts from this event are consistent with its magnitude being similar to our M_{TOL} for nuisance.

4.3 Comparison with Castor

We also compare our M_{TOL} estimates with experience with one of the most notable examples of an offshore facility being negatively impacted by induced seismicity. In doing so, we note that our M_{TOL} estimates are based on ground motion models and fragility models that were not calibrated for the area in question, and so an exact match between modelled and observed impacts should not be expected.

As described in our introduction, the Castor gas storage site was located approximately 20 km from the eastern coast of Spain. It experienced three earthquakes with M 4.1 – 4.2 during its first weeks of operation (Ruiz Barajas et al., 2017). These events were felt by the public along the coastline. The resulting public concern led to significant protests such that injection was paused, and eventually the entire project was closed down. We are not aware of any reports of damage from the Castor seismicity.

From our relationships between M_{TOL} and the distance to the coast shown in Figure 9, for an activity that is located 20 km from the coast, we expect an M_{TOL} for nuisance of M 3.2, and an M_{TOL} for damage of M 4.1. Our M_{TOL} value for nuisance is consistent with what occurred at Castor since the events, which were significantly larger than our M_{TOL}, caused nuisance to the nearby population along the coast such that the project was eventually abandoned. The largest of the Castor events just equalled our M_{TOL} estimate for damage. Given the inherent variability in ground motions and seismic impacts, the absence of reported damage from the Castor events is consistent with our model outcomes.

4.4 M_{TOL} and induced seismicity management

The M_{TOL} values that we have estimated represent the threshold of seismicity that would become intolerable. The M_{TOL} values should inform induced seismicity management, but they do not represent thresholds at which operations should be adjusted in order to mitigate induced seismicity risk. If operations are not adjusted until after M_{TOL} is reached, then magnitude jumps and trailing events could produce levels of seismicity that significantly exceed M_{TOL} (Verdon and Bommer, 2021). Hence, actions to mitigate induced seismicity must be taken before induced event magnitudes reach M_{TOL}.

If a TLS is adopted to manage induced seismicity, then the red threshold, M_{RED}, must be set at a value lower than M_{TOL}. Statistical considerations of induced seismicity sequences (Schultz et al., 2020b) and observations of large numbers of sequences in practice (Verdon and Bommer, 2021; Watkins et al., 2023) have indicated that TLS thresholds for long-term, low-pressure injection (such as CCS) should be set approximately 1.5 to 2 magnitude units below M_{TOL}. This gap is needed to ensure that jumps and trailing events as magnitudes approach M_{RED} due not exceed M_{TOL}.

For adaptive measures where magnitude forecasting models are used to manage induced seismicity, a sufficient number of smaller events are required for model calibration. Many modelling strategies require an estimate of the Gutenberg-Richter *b*-value, which in turn requires a bandwidth of several units of magnitude to produce an accurate estimate (Roberts et al., 2015). Furthermore, modelled increases in magnitude of 1 to 2 orders are commonly produced by such models (e.g., Schultz et al., 2022; Verdon et al., 2024; Verdon and Eisner, 2024). Monitoring systems must therefore be capable of detecting earthquake magnitudes that are significantly lower than M_{TOL}, by as much as two or three orders of magnitude, to enable the use of an ATLS strategy.

Given our estimates for M_{TOL}, it is of interest to examine whether the existing UK national seismic monitoring network provides sufficient monitoring capability to manage induced seismicity at offshore CCS sites. The detection capability of the UK's national seismic network is shown in Baptie (2021). Approximate ranges of detection capability for the areas in which CCS licenses are held are as follows: East Irish Sea: $1.5 \leq M_D \leq 2.0$; English Channel: $1.5 \leq M_D \leq 2.0$; southern North Sea: $2.0 \leq M_D \leq 2.5$; central North Sea: $2.25 \leq M_D \leq 2.75$; northern North Sea: $2.5 \leq M_D \leq 3.0$. The M_{TOL} values for nuisance in these areas are: East Irish Sea: $3.0 \leq M_{TOL} \leq 3.5$; English Channel: $3.25 \leq M_{TOL} \leq 3.75$; southern North Sea: $3.25 \leq M_{TOL} \leq 4.25$; central North Sea: $4.25 \leq M_{TOL} \leq 4.75$; northern North Sea: $4.75 \leq M_D \leq 5.25$.

Hence, for the central and northern North Sea, the detection thresholds are 2 or more magnitude units lower than M_{TOL}, implying that sufficient earthquake detection capability is available to provide useful observations to manage induced seismicity risk. However, for the southern North Sea, East Irish Sea and English Channel, the difference between M_D and M_{TOL} is roughly 1.25 to 1.5 magnitude units. As such, modest improvements to existing monitoring capabilities for these areas may be warranted to adequately manage the risks posed by induced seismicity.

Improvements in monitoring capabilities may be required to reduce location uncertainties – without accurate locations it may be difficult to reliably distinguish induced events from natural earthquakes. Furthermore, in addition to managing the risks posed by large induced seismic events, operators may wish to install improved passive seismic monitoring capabilities around their CCS sites for other purposes, such as to understand the geomechanical response of the reservoir to CO_2 injection and to detect fracturing in the caprock, (e.g., Verdon et al., 2011, 2013; Stork et al., 2015).

5. CONCLUSIONS

The risks of induced seismicity during injection operations are typically managed by observing events and adjusting activities accordingly. Decisions can be made via a TLS, or by using forecasting models that estimate upcoming magnitudes. In either case, decisions should be made based on an understanding of what earthquake magnitude will be tolerable to nearby populations. This tolerability can be defined based on the likelihood of experiencing nuisance or of experiencing damage.

In this study we have calculated tolerability thresholds for the CCS operations that are expected to commence in the seas around the UK in the coming decade. To do so, we adapted the method that was developed by Schultz et al. (2023) for application to UK shale gas operations. Ground motions were estimated over grids of given magnitude at a given location. For a specific level of ground motion, the likelihood of experiencing nuisance or damage was estimated from fragility functions. The numbers of affected households affected by a given impact were then estimated based on the population at a given point. The thresholds for tolerability were defined based on past observations of induced event impacts in the UK, and the tolerance, or lack of thereof, for these events as evidenced by the public and regulatory responses.

Our primary results, the thresholds for tolerability mapped in Figures 5 – 8, can be used by the holders of CCS license blocks around the UK (and the regulators thereof) as a key input to the design of induced seismicity mitigation strategies for their upcoming projects.

We found that the first order control on M_{TOL} is the distance from the coast. The population density along the coast and V_{S30} values also play a relatively smaller (but still important) role. As such, the M_{TOL} values for future offshore CCS sites will depend on their location. Sites near to a densely populated coast, such as in the East Irish Sea, English Channel, and southern North Sea, may exceed the threshold for tolerance to nuisance at magnitudes as low as M 3.0. Sites in the central and northern North Sea will have significantly higher thresholds for tolerability. We sense-checked our M_{TOL} estimates against macroseismic impacts observed for past historical earthquakes occurring in the seas around the UK, finding that our thresholds for nuisance and damage are consistent with the magnitudes of past earthquakes that have been widely felt and/or caused damage.

To manage induced seismicity risks, earthquake monitoring systems must be able to detect magnitudes significantly lower than M_{TOL}. By detecting smaller events, an operator can act to mitigate induced seismicity, guided either by a TLS or by statistics-based forecasting models that are calibrated with smaller events. In the central and northern North Sea, earthquake detection capabilities with the existing BGS national seismic network are more than two orders of magnitude smaller than M_{TOL}. However, in the East Irish Sea, English Channel, and southern North Sea, where M_{TOL} values are smaller, the detection capability is in some places within 1.25 magnitude units of M_{TOL}. In these areas, modest improvements in monitoring capabilities may be required to adequately manage induced seismicity risks as the CCS industry develops.

References

Baptie, B., 2021. Earthquake Seismology 2020/2021. British Geological Survey Open Report, OR/21/033.

BEIS, 2019. Government ends support for fracking: Press Release from the UK Department of Business, Energy and Industrial Strategy. Available at: https://www.gov.uk/government/news/government-ends-support-for-fracking (last accessed 02/05/2024).

BEIS, 2021. Net zero strategy: Build back greener. Department for Business, Energy and Industrial Strategy, London. ISBN 978-1-5286-2938-6. Available at: https://www.gov.uk/government/publications/net-zero-strategy (last accessed 02/05/2024).

BGS, 2010. UK historical earthquake database: British Geological Survey. Available at: http://quakes.bgs.ac.uk/historical/ (last accessed 03/07/2024).

Bommer, J.J., and J.P. Verdon, 2024. The maximum magnitude of natural and induced earthquakes: ESS Open Archive, doi: 10.22541/essoar.171826172.29972480/v1.

Bommer, J.J., S. Oates, J.M. Cepeda, C. Lindholm, J.F. Bird, R. Torres, G. Marroquín, J. Rivas, 2006. Control of hazard due to seismicity induced by a hot fractured rock geothermal project: Engineering Geology 83, 287-306.

Bommer, J.J., H. Crowley, R. Pinho, 2015. A risk-mitigation approach to the management of induced seismicity: Journal of Seismology 19, 623-464.

BSI, 2014. Code of practice for noise and vibration control on construction and open sites – Part 2: Vibration. British Standards Institution, London. BS 5228-2:2009+A1:2014.

Campbell, N.M., M. Leon-Corwin, L.A. Ritchie, J. Vickery, 2020. Human-induced seismicity: risk perceptions in the state of Oklahoma: The Extractive Industries and Society 7, 119-126.

CBO, 2023. Carbon capture and storage in the United States: Congressional Budget Office Publication 59345. Available at: https://www.cbo.gov/system/files/2023-12/59345-carbon-capture-storage.pdf (last accessed 02/05/2024).

Cesca, S., D. Stich, F. Grigoli, A. Vuan, J.Á. López-Comino, P. Niemz, E. Blanch, T. Dahm, W.L. Ellsworth, 2021. Seismicity at the Castor gas reservoir driven by pore pressure diffusion and asperities loading: Nature Communications 12, 4783.

Clarke, H., L. Eisner, P. Styles, P. Turner, 2014. Felt seismicity associated with shale gas hydraulic fracturing: the first documented example in Europe: Geophysical Research Letters 41, 8308-8314

Clarke, H., J.P. Verdon, T. Kettlety, A.F. Baird, J-M. Kendall, 2019. Real time imaging, forecasting and management of human-induced seismicity at Preston New Road, Lancashire, England: Seismological Research Letters 90, 1902-1915.

Dando, B.D.E., B.P. Goertz-Allmann, D. Kühn, N. Langet, A.M. Dichiarante, V. Oye, 2021. Relocating microseismicity from downhole monitoring of the Decatur CCS site using a modified double-difference algorithm: Geophysical Journal International 227, 1094-1122.

Eaton, D.W., and R. Schultz, 2018. Increased likelihood of induced seismicity in highly overpressured shale formations: Geophysical Journal International 214, 751-757.

Eaton, D.W., N. Igonin, A. Poulin, R. Weir, H. Zhang, S. Pellegrino, G. Rodriguez, 2018. Induced seismicity characterization during hydraulic-fracture monitoring with a shallow-wellbore geophone array and broadband sensors: Seismological Research Letters 89, 1641-1651.

Edwards, B., H. Crowley, R. Pinho, J.J. Bommer, 2021. Seismic hazard and risk due to induced earthquakes at a shale gas site: Bulletin of the Seismological Society of America 111, 875-897.

Esposito, S. and I. Iervolino, 2012. Spatial correlation of spectral acceleration in European data: Bulletin of the Seismological Society of America 102, 2781-2788.

Evensen, D., A. Varley, L. Whitmarsh, P. Devine-Wright, J. Dickie, P. Bartie, H. Napier, I. Mosca, C. Foad, S. Ryder, 2022. Effect of linguistic framing and information provision on attitudes towards induced seismicity and seismicity regulation: Scientific Reports 12, 11239.

Goertz-Allmann, B.P., N. Langet, K. Iranpour, D. Kühn, A. Baird, S. Oates, C. Rowe, S. Harvey, V. Oye, H. Nakstad, 2024. Effective microseismic monitoring of the Quest CCS site, Alberta, Canada: International Journal of Greenhouse Gas Control 133, 104100.

Galloway, D.D., 2012. Bulletin of British Earthquakes 2011: British Geological Survey Internal Report, OR/12/041.

Galloway, D.D., 2014. Bulletin of British Earthquakes 2013: British Geological Survey Internal Report, OR/14/062.

Galloway, D.D., 2016. Bulletin of British Earthquakes 2015: British Geological Survey Internal Report, OR/16/012.

Galloway, D.D., 2018. Bulletin of British Earthquakes 2017: British Geological Survey Internal Report, OR/18/015.

Galloway, D.D., 2023. The British Geological Survey Earthquake Bulletin for 2022: British Geological Survey Internal Report, OR/23/005.

Hallo, M., I. Oprsal, L. Eisner, M.Y. Ali, 2014. Prediction of magnitude of the largest potentially induced seismic event: Journal of Seismology 18, 421-431.

Häring, M.O., U. Schanz, F. Ladner, B.C. Dyer, 2008. Characterisation of the Basel 1 enhanced geothermal system: Geothermics 37, 469-495.

Heath, D.C., D.J. Wald, C.B. Worden, E.M. Thompson, G.M. Smoczyk, 2020. A global hybrid Vs30 map with a topographic slope–based default and regional map insets: Earthquake Spectra 36, 1570-1584.

Hicks, S.P., J.P. Verdon, B. Baptie, R. Luckett, Z.K. Mildon, T. Gernon, 2019. A shallow earthquake swarm close to hydrocarbon activities: discriminating between natural and induced causes for the 2018-19 Surrey, UK earthquake sequence: Seismological Research Letters 90, 2095-2110.

Jones, A.C., and A.J. Lawson, 2022. Carbon capture and sequestration (CCS) in the United States: Congressional Research Service, Washington D.C., USA. R44902.

Kendall, J-M. A. Butcher, A.L. Stork, J.P. Verdon, R. Luckett, B.J. Baptie, 2019. How big is a small earthquake? Challenges in determining microseismic magnitudes: First Break 37, 51-56

Kettlety, T., J.P. Verdon, A. Butcher, M. Hampson, L. Craddock, 2021. High-resolution imaging of the M_L 2.9 August 2019 earthquake in Lancashire, United Kingdom, induced by hydraulic fracturing during Preston New Road PNR-2 operations: Seismological Research Letters 92, 151-169.

Korswagen, P., M. Longo, E. Meulman, L. Licciardello, M. Sousamli, 2019. Damage sensitivity of Groningen masonry – experimental and computational studies: Part 2, NAM Report by Delft University of Technology.

Kwiatek, G., T. Saamo, T. Ader, F. Bluemle, M. Bohnhoff, M. Chendorain, G. Dresen, P. Heikkinen, I. Kukkonen, P. Leary, M. Leonhardt, P. Malin, P. Martinez-Garzon, K. Passmore, P. Passmore, S. Valenzuela, C. Wollin, 2019. Controlling fluid-induced seismicity during a 6.1-km-deep geothermal stimulation in Finland: Science Advances 5, eaav7224.

Langenbruch, C., M. Weingarten, M.D. Zoback, 2018. Physics-based forecasting of man-made earthquake hazards in Oklahoma and Kansas: Nature Communications 9, 3946.

Lee, K.K., W.L. Ellsworth, D. Giardini, J. Townend, S. Ge, T. Shimamoto, I-W. Yeo, T-S. Kang, J. Rhie, D-H. Sheen, C. Chang, J-U. Woo, C. Langenbruch, 2019. Managing injection-induced seismic risks: Science 364, 730-732.

Lei, X., Z. Wang, J. Su, 2019. The December 2018 M_L 5.7 and January 2019 M_L 5.3 earthquakes in south Sichuan Basin induced by shale gas hydraulic fracturing: Seismological Research Letters 90, 1099-1110.

Mancini, S., M.J. Werner, M. Segou, B. Baptie, 2021. Probabilistic forecasting of hydraulic fracturing-induced seismicity using an injection-rate driven ETAS model: Seismological Research Letters 92, 3471-3481.

Mignan, A., M. Broccardo, S. Wiemer, D. Giardini, 2017. Induced seismicity closed-form traffic light system for actuarial decision-making during deep fluid injections: Scientific Reports 7, 13607.

Musson, R.M.W., 2007. British earthquakes: Proceedings of the Geologists Association 118, 305-337.

Nantanoi, S., G. Rodríguez-Pradilla, J.P. Verdon, 2022. 3D-Seismic interpretation and fault slip potential analysis from hydraulic fracturing in the Bowland Shale, UK: Petroleum Geoscience 28, petgeo2021-057.

Neilson, G., R.M.W. Musson, P.W. Burton, 1986. Macroseismic reports on historical British earthquakes XI: 1931 June 7 North Sea: British Geological Survey Global Seismology Report 280.

OCC, 2016. Media advisory - Regional earthquake response plan for western Oklahoma: Oklahoma Corporation Commission, Oklahoma City, OK. Retrieved from https://oklahoma.gov/content/dam/ok/en/occ/documents/ajls/news/2016/02-16-16westernregionalplan.pdf (last accessed 02/05/2024).

Roberts, N.S., A.F. Bell, I.G. Main, 2015. Are volcanic seismic b-values high, and if so when? Journal of Volcanology and Geothermal Research 308, 127-141.

Rodríguez-Pradilla, G., and J.P. Verdon, 2024. Quantifying the variability in fault density across the UK Bowland Shale, with implications for induced seismicity hazard: Geomechanics for Energy and the Environment 38, 100534.

Rose, A., J. McKee, M. Urban, E. Bright, K. Sims, 2019. LandScan 2018 high-resolution global population data set: Oak Ridge National Laboratory, Oak Ridge, TN, United States.

Ruiz Barajas, S., N. Sharma, V. Convertito, A. Zollo, B. Benito, 2017. Temporal evolution of a seismic sequence induced by a gas injection in the Eastern coast of Spain: Scientific Reports 7, 2901.

Sargeant, S.L., and R.M.W. Musson, 2009. Rotational earthquake effects in the United Kingdom: Bulletin of the Seismological Society of America 99, 1475-1479.

Schultz, R., H. Corlett, K. Haug, K. Kocon, K. MacCormack, V. Stern, T. Shipman, 2016. Linking fossil reefs with earthquakes: geologic insight to where induced seismicity occurs in Alberta: Geophysical Research Letters 43, 2534-2542.

Schultz, R. R.J. Skoumal, M.R. Brudzinski, D. Eaton, B. Baptie, W. Ellsworth, 2020a. Hydraulic fracturing-induced seismicity: Reviews of Geophysics 58, e2019RG000695.

Schultz, R., G. Beroza, W. Ellsworth, J. Baker, 2020b. Risk-informed recommendations for managing hydraulic fracturing-induced seismicity via Traffic Light Protocols: Bulletin of the Seismological Society of America 110, 2411-2422.

Schultz, R., G.C. Beroza, & W.L. Ellsworth, 2021a. A risk-based approach for managing hydraulic fracturing–induced seismicity: Science 372, 504-507.

Schultz, R., G.C. Beroza, & W.L. Ellsworth, 2021b. A strategy for choosing red-light thresholds to manage hydraulic fracturing induced seismicity in North America: Journal of Geophysical Research: Solid Earth 126, e2021JB022340.

Schultz, R., V. Quitoriano, D.J. Wald, G.C. Beroza, 2021c. Quantifying nuisance ground motion thresholds for induced earthquakes: Earthquake Spectra 37, 789-802.

Schultz, R., Ellsworth, W. L., Beroza, G. C. 2022. Statistical bounds on how induced seismicity stops. Scientific Reports: 12, 1184.

Schultz, R., B. Baptie, B. Edwards, S. Wiemer, 2023. Red-light thresholds for induced seismicity in the UK: Seismica 2, 1086.

Schultz, R., A.P. Rinaldi, P. Roth, H. Madritsch, S. Wiemer, 2024a. Pre-screening of induced seismicity risks for CO_2 injection at Trüllikon, Switzerland: International Journal of Greenhouse Gas Control 138, 104239.

Schultz, R., 2024b. Inferring maximum magnitudes from the ordered sequence of large earthquakes. Philosophical Transactions of the Royal Society A: 382, 20230185.

Segall, P., 1989. Earthquakes triggered by fluid extraction: Geology 17, 942-946.

Stork A.L., J.P. Verdon, J-M. Kendall, 2015. The microseismic response at the In Salah Carbon Capture and Storage (CCS) site: International Journal of Greenhouse Gas Control 32, 159-171.

van de Graaff, W.J.E., L. van Geuns, T. Boersma, 2018. The termination of Groningen gas production – background and next steps: Columbia School of International and Public Affairs Center on Global Energy Policy.

Verdon, J.P., 2014. Significance for secure CO_2 storage of earthquakes induced by fluid injection: Environmental Research Letters 9, 064022.

Verdon, J.P., 2016. Using microseismic data recorded at the Weyburn CCS-EOR site to assess the likelihood of induced seismic activity: International Journal of Greenhouse Gas Control 54, 421-428.

Verdon, J.P. and J.J. Bommer, 2021. Green, yellow, red, or out of the blue? An assessment of Traffic Light Schemes to mitigate the impact of hydraulic fracturing-induced seismicity: Journal of Seismology 25, 301-326.

Verdon, J.P., and G. Rodríguez-Pradilla, 2023. Assessing the variability in hydraulic fracturing-induced seismicity occurrence between North American shale plays: Tectonophysics 859, 229898.

Verdon, J.P., and L. Eisner, 2024. An empirically constrained forecasting strategy for induced earthquake magnitudes using extreme value theory: Seismological Research Letters, in press. DOI: 10.1785/0220240061.

Verdon, J.P., J-M. Kendall, D.J. White, D.A. Angus, 2011. Linking microseismic event observations with geomechanical models to minimise the risks of storing CO_2 in geological formations: Earth and Planetary Science Letters 305, 143-152.

Verdon, J.P., J-M. Kendall, A.L. Stork, R.A. Chadwick, D.J. White, R.C. Bissell, 2013. A comparison of geomechanical deformation induced by 'megatonne' scale CO_2 storage at Sleipner, Weyburn and In Salah: Proceedings of the National Academy of Sciences 110, E2762-E2771.

Verdon, J.P., B. Pullen, G. Rodriguez-Pradilla, 2024. Growth and stabilisation of induced seismicity rates during long-term, low pressure fluid injection: Philosophical Transactions of the Royal Society A 382, 20230183.

Versey, H.C., 1939. The North Sea earthquake of 1931 June 7: Geophysical Supplements to the Monthly Notices of the Royal Astronomical Society 4, 416-423.

Wald, D.J., V. Quitoriano, C.B. Worden, M. Hopper, J.W. Dewey, 2012. USGS "Did You Feel It?" internet-based macroseismic intensity maps: Annals of Geophysics 54, 688-707.

Watkins, T.J.M., J.P. Verdon, G. Rodríguez-Pradilla, 2023. The temporal evolution of induced seismicity sequences generated by long-term, low pressure fluid injection: Journal of Seismology 27, 243-259.

Wozniakowska, P., and D.W. Eaton, 2020. Machine learning-based analysis of geological susceptibility to induced seismicity in the Montney Formation, Canada: Geophysical Research Letters 47, e2020GL089651.

Zang, A., V. Oye, P. Jousset, N. Deichmann, R. Gritto, A. McGarr, E. Majer, D. Bruhn, 2014. Analysis of induced seismicity in geothermal reservoirs - an overview: Geothermics 52, 6-21.

Zhou, W., F. Lanza, I. Grigoratos, R. Schultz, J. Cousse, E. Trutnevyte, A. Muntendam-Bos, S. Wiemer, 2024. Managing induced seismicity risks from enhanced geothermal systems: a good practice guideline: Reviews of Geophysics, in press. DOI: 10.1029/2024RG000849.

Zoback, M.D., and S.M. Gorelick, 2012. Earthquake triggering and large-scale geologic storage of carbon dioxide: Proceedings of the National Academy of Sciences 109, 10164-10168.